Small Infrared Target Detection Based on Weighted Local Difference Measure

He Deng, Xianping Sun, Maili Liu, Chaohui Ye, and Xin Zhou

***Abstract*—Against an intricate infrared cloudy-sky background, jamming objects such as the edges of clouds in the scene have a similar thermal intensity measure with respect to the background as small targets. This may cause high false alarm rates and low probabilities of detection according to conventional small target detection methods. In this paper, we propose a weighted local difference measure (WLDM)-based scheme for the detection of small targets against various complex cloudy-sky backgrounds. Initially, a WLDM map is achieved to simultaneously enhance targets and suppress background clutters and noise. In this way, the true targets can be easily separated from jamming objects. After that, a simple adaptive threshold is used to segment the targets. More than 460 infrared small target images against diverse intricate cloudy-sky backgrounds were utilized to validate the detection capability of the WLDM-based method. Experimental results demonstrate that the proposed algorithm not only works more robustly for different cloudy-sky backgrounds, target movements, and signal-to-clutter ratio (SCR) values but also has a better performance with regard to the detection accuracy, in comparison to traditional baseline methods. In particular, the proposed method is able to significantly improve SCR values of the images.**

***Index Terms*—Cloudy-sky background, infrared image, small target detection, weighted local difference measure (WLDM).**

I. Introduction

TARGET detection is widely applied in various fields, such as aerospace, remote sensing, and medical imaging [1]–[3]. In comparison to radar systems and visible light systems, infrared search and tracking (IRST) systems have some advantages such as high resolution, strong smoke penetration abilities, and simple structure. Consequently, IRST systems have received much attention [4]–[6]. The detection of a target with unknown position and velocity is crucial in IRST applications to early warn incoming targets (e.g., airplanes and missiles) from a long distance [7]–[12]. Because of the long imaging distance, a target is with small size without concrete shape and texture, and it is usually buried in low signal-to-clutter ratio (SCR) background clutters and noise [1]. Although extensive research efforts have been focused on this field in past decades, small target detection against complicated backgrounds still remains an open issue.

Current state-of-the-art small target detection methods can be simply categorized into two classes: track-before-detect (TBD) methods [7] and detect-before-track (DBT) methods [8]. The TBD methods usually process a number of frames to estimate targets while necessitating some prior knowledge of the target [1]. The 3-D matched (directional) filter [13] can detect moving targets with a constant velocity, which demands the knowledge about the target shape and velocity. The 3-D double directional filter [14] and improved 3-D directional filter [15] are proposed to improve the ability of detecting weak targets. These methods require the prior knowledge about the maximum target velocity. Moreover, some methods based on modified partial differential equation [16] or support vector machines [17] have been proposed, where the background is suppressed in a single image and, then, false alarms are deleted by using the multiframe accumulation or autocorrelation.

Compared with TBD methods, DBT methods have several merits, such as the shorter computation time and fewer requirements of assumptions and/or prior knowledge. Thus, this method has been drawing a lot of attention [1]–[5], [18]–[20]. The finite or infinite impulse response filter and the space-time maximum likelihood algorithms [21] can suppress backgrounds with the assumption of the short-time stationarity. Methods such as the top-hat [8], median, Maxmean, and Maxmedian filters [22] are widely used to reduce background clutters. However, the top-hat method is sensitive to noise [1], [4]. Lately, the adaptive fractional Fourier transform [23] and Radon-fractional Fourier transform [24] have been presented to detect radar targets. However, their algorithm complexities are expensive. Moreover, classification-based methods are helpful to remove clutter points [19], such as the manifold learning [25], nearest neighbor classifier [26], and learning-based neural network [27]. There are still many other algorithms for detecting small targets, such as methods based on the trifeature-based detector [11], statistical regression [12], or biological vision [28]. However, against intricate cloudy-sky backgrounds, edges of clouds have similar thermal intensities to that of small targets, which may arouse high false alarm rates (FAs). Hence, it is still a challenge to detect small targets embedded in complicated and noisy cloudy-sky backgrounds.

Manuscript received September 10, 2015; revised January 12, 2016; accepted February 29, 2016. Date of publication April 27, 2016; date of current version May 24, 2016. This work was supported in part by the Natural Science Foundation of China under Grants 61471355 and 81227902 and in part by the China Postdoctoral Science Foundation under Grants 2014M560636 and 2015T80856.

H. Deng is with the State Key Laboratory of Magnetic Resonance and Atomic and Molecular Physics, National Center for Magnetic Resonance in Wuhan, Wuhan Institute of Physics and Mathematics, Chinese Academy of Sciences, Wuhan 430071, China, and also with the Department of Information Technology, Central China Normal University, Wuhan 430079, China.

X. Sun, M. Liu, C. Ye, and X. Zhou are with the State Key Laboratory of Magnetic Resonance and Atomic and Molecular Physics, National Center for Magnetic Resonance in Wuhan, Wuhan Institute of Physics and Mathematics, Chinese Academy of Sciences, Wuhan 430071, China (e-mail: xinzhou@wipm.ac.cn).

Color versions of one or more of the figures in this paper are available online at http://ieeexplore.ieee.org.

Digital Object Identifier 10.1109/TGRS.2016.2538295

In order to detect a small infrared target buried in an intricate cloudy-sky background, it is inspiring to adopt the concepts of local difference/mutation [29]–[31]. The reason is that a small target often occupies several pixels in an image, which causes a considerable change of textural characteristics in a local region rather than the whole image plane. Recently, target detection methods based on the local difference/mutation have attracted much attention, for example, the sparse ring representation [9], probabilistic principal component analysis [29], kernel-based nonparametric regression [12], local contrast measure (LCM) [2], local mutation weighted information entropy (LMWIE) [30], and average gray absolute difference maximum (AGADM) map [31]. Consequently, the local difference/mutation model can guide the design of a new algorithm. Noticed that a small target concentrates in a small, homogeneous, and compact region, and it has a conspicuous discontinuity with its neighboring background areas [27], [31], where the discontinuity is essentially involved in ascertaining the property of average gray difference based on the neighboring pixels [31]. Moreover, the target size may vary due to different types of targets, imaging distances, environments, and so on [1]. Therefore, we conceive a novel multiscale measure to represent the local difference between the small target and background clutters. After the measure, the local region whose difference is larger than a given threshold in some scale may be a position where the target emerges. With these considerations in mind, we design a method inspired by the local difference or mutation model to detect small infrared targets against diverse complex and noisy cloudy-sky backgrounds in this paper.

The contributions of this paper can be summarized as follows: 1) A multiscale local difference contrast is presented to represent the discontinuity between the target region and the surrounding background clutters. This contrast can enlarge the original brightness difference. In this way, the target is well enhanced. 2) A weighted local difference measure (WLDM) is proposed to separate the true target from jamming objects like the edges of clouds. This measure can simultaneously enhance the target and suppress background clutters. In particular, it can significantly improve SCR values of the image. These recently proposed techniques can guarantee to efficiently process low SCR infrared images against various complex and noisy cloudy-sky backgrounds. We use real data to test the proposed method. Experimental results demonstrate that, against diverse intricate cloudy-sky backgrounds, our method is simple and effective with respect to (wrt) detection accuracy. In particular, it shows a significant superiority over conventional baseline methods in terms of the SCR values and background suppression factor (BSF) values.

The organization of the remainder of this paper is as follows. In Section II, we explain the target detection method based on the novel measure in detail. In Section III, we give extensive data experimental results and discussions. Conclusion and perspectives are given in Section IV.

II. Small Target Detection Based on WLDM

In this section, we introduce a new scheme for the detection of a small infrared target embedded in cloudy-sky backgrounds with clutters and noise. This scheme weights a multiscale local difference contrast by the modified local entropy to separate the true target from jamming objects and subsequently utilizes a simple threshold to detect the target in the filtered result. It is good at suppressing various intricate cloudy-sky backgrounds and improving SCR values of the image.

A. Multiscale Local Difference Contrast

A viewpoint of human recognition of a small infrared target from a natural scene is that the target region has conspicuous discontinuity with the surrounding background [2], [31]. The target region is generally viewed as a small, homogeneous, and compact area [27], and the discontinuity is essentially involved in determining the property of average gray difference based on the neighboring pixels [31]. Hence, the most dissimilar point according to a specific measure of average gray difference in the scene is considered as a target. Moreover, the target size is constantly changing owing to the change of imaging distance [1], [2]. This should be pondered in the design of the specific measure as well. Ideally, the size of a window (viz., target region) should be the same as the target size, which suggests that the size of the window should change as the target size changes. However, some prior knowledge such as the target size or imaging distance is seldom obtained in real applications. In this case, a multiscale local difference contrast is presented to represent the discontinuity between the target region and the surrounding background clutters.

Given a pixel point (x, y) in an image, its kth neighborhood is defined as follows:

$$\Omega_k = \{(p,q)\,|\max(|p-x|,|q-y|) \le k\}, k = 1, 2, \ldots, L \tag{1}$$

where L is a positive integer.

The average gray value of the kth neighborhood is

$$A_k(x,y) = \frac{1}{N_k} \sum_{(s,t)\in\Omega_k} f(s,t) \tag{2}$$

where N_k denotes the number of pixels included in the kth neighborhood Ω_k and $f(s,t)$ denotes the gray value at the pixel point (s,t) contained in Ω_k.

Thus, the kth local difference contrast is expressed by the following formula:

$$\begin{aligned} C_k(x,y) &= \frac{|A_k(x,y) - A_L(x,y)|^2}{|\alpha_{\max} - \alpha_{\min}|^2} \\ \text{where } \alpha_{\max} &= \max\{A_1(x,y), A_2(x,y), \ldots, A_L(x,y)\} \\ \text{and } \alpha_{\min} &= \min\{A_1(x,y), A_2(x,y), \ldots, A_L(x,y)\}. \end{aligned} \tag{3}$$

Accordingly, the multiscale local difference contrast is

$$C(x,y) = \max\{C_1(x,y), C_2(x,y), \ldots, C_{L-1}(x,y), 0\}. \tag{4}$$

For each pixel point in a given scale, its multiscale local difference contrast can be acquired in this way. When the window in (1)–(4) moves in the image from left to right and from top to down, we will achieve a matrix of multiscale local difference

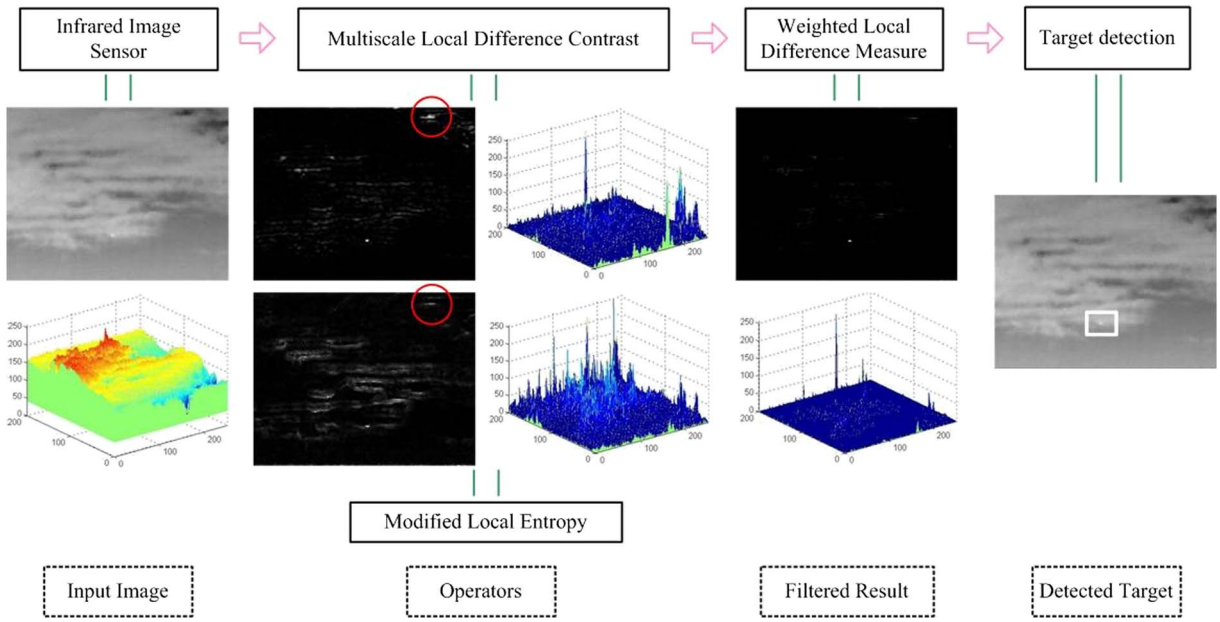

Fig. 1. Proposed small infrared target detection system.

contrast. Each element in the matrix represents the maximal discontinuity between the current region and the surrounding neighborhoods.

B. WLDM

For a representative small target image against complicated cloudy-sky background, the map of multiscale local difference contrast and the corresponding 3-D surface are shown in Fig. 1, where the largest scale L in (4) is chosen as 4. The map suggests that the target is nicely enhanced. However, it can be seen that there exist some clutters and noise residual although a mass of background clutters and noise are well suppressed. The existence of residues is due to the fact that, against an intricate cloudy-sky background, the edges of clouds (viz., the border areas between the sky and cloud) have similar thermal intensity measures wrt the background as small targets. These clutters and noise residual possibly have an effect on the performance of the multiscale local difference contrast because fewer residues determine lower FAs under the same probability of detection (PD) [1].

Noticed that a small target usually emerges as a small bright region in an infrared image [8]. Such target can be isolated from the background based on the difference of gray values between the target and background. Since the information entropy can represent the complex degree of gray value distribution upon an image, the modified local entropy is presented in [30] to emphasize the contribution of those components with high gray values to the entropy of an image.

For an image with a size of $M \times N$, $f(x, y)$ is assumed as the gray value at the pixel point (x, y), and its neighborhood is defined as

$$\Theta = \{(p, q) \,||p - x| \leq m, \text{ and } |q - y| \leq n\} \tag{5}$$

where m and n are positive integers. If the neighborhood contains m_1 kinds of gray values, f_i, $i = 1, 2, \ldots, m_1$, the modified local entropy will be expressed as

$$W(x, y) = -\sum_{i=1}^{m_1} (f_i - f(x, y))^2 p_i \log_2 p_i, \text{ where } p_i = \frac{n_i}{M \times N} \tag{6}$$

where p_i, $i = 1, 2, \ldots, m_1$, is the probability density function of the ith gray level and n_i is the number of pixels of the ith gray level. For the representative small target image, the map of modified local entropy is shown in Fig. 1, where the scales in (5) and (6) are $m = n = 2$.

Fig. 1 suggests that the target is enhanced by using the modified local entropy or multiscale local difference contrast. However, there exist different degrees of clutters and noise residual in the two preliminary results, owing to the effect of cloud edges (e.g., the areas marked by red circles in Fig. 1). If the multiscale local difference contrast is weighted by the modified local entropy, the impact caused by the clutters and noise residual will be greatly offset (see Fig. 1). Consequently, a WLDM is proposed, aiming to improve the separability for the cases where jamming objects in the scene have similar thermal intensity measures as the target.

Therefore, the WLDM at the point (x, y) can be achieved via the following formula:

$$wC(x, y) = W(x, y) \times C(x, y) \tag{7}$$

where $W(x, y)$ and $C(x, y)$ denote the modified local entropy and the multiscale local difference contrast at the point (x, y). This algorithm can make the WLDM traverse the whole image and then achieve a WLDM map, as shown in Fig. 1. Like this, the clutters and noise residual are well eliminated, which indicates that the WLDM can improve the adaptability and robustness of the multiscale local difference contrast.

C. WLDM-Based Small Target Detection Method

As mentioned before, a small target is discontinuous with its neighboring areas, while the background is consistent with its neighboring areas [2], [31]. The WLDM map can enlarge the discontinuity of the target region from its neighboring areas and effectively suppress the background clutters and noise (see Fig. 1). Therefore, we believe that, if a WLDM map is achieved, it is likely that the most salient point in the scene is a target.

According to this fact, the WLDM-based small infrared target detection method is described in Algorithm 1, where the size of an image is $M \times N$, wC is the WLDM, C is the multiscale local difference contrast, W is the modified local entropy, T is the threshold to segment the target, $f(x,y)$ is the gray value at the pixel point (x,y), f_i is the ith gray level, mn and sm are the mean and maximum values of the WLDM map, and λ is a constant, respectively. In general, the user can manually and experimentally select the parameter λ, the maximum window size to compute the multiscale local difference contrast in (4), and the window size to compute the weights in (6) for practical design requirements. In our experiments, λ is chosen within an interval [0.3, 0.6]. In order to intuitively show the proposed method, the proposed small infrared target detection system is given in Fig. 1.

Algorithm 1 WLDM-based small infrared target detection method.

Input: One frame.
Output: Target position.
1) Enough scale L of the window are given for the computation of multiscale local difference contrast.
2) Enough scales m, n of the window are given for the computation of modified local entropy, and the number of gray levels contained in the window is assumed as m_1.
3) **for** $x = 1{:}M$ **do**
4) **for** $y = 1{:}N$ **do**
5) Obtain a set of neighborhoods at pixel point (x,y):

$$\{\Omega_k \,|\Omega_k \subseteq \Omega_L, k \in \{1,2,\ldots,L\}\}.$$

6) **for** $k = 1,2,\ldots,L$, **do**
Compute the kth local difference contrast according to (2) and (3).
7) **end for**
8) Obtain the multiscale local difference contrast:

$$C(x,y) = \max\{C_1(x,y),\ C_2(x,y),\ldots,C_{L-1}(x,y),0\}.$$

9) **for** $i = 1{:}m_1$ **do**

$$\omega_i = -\left(f_i - f(x,y)\right)^2 p_i \log_2 p_i.$$

10) **end for**
11) Obtain the modified local entropy: $W(x,y) = \sum_{i=1,\ldots,m1} \omega_i$.
12) Compute the WLDM:

$$wC(x,y) = W(x,y) \times C(x,y).$$

13) Replace the gray value at the pixel point with $wC(x,y)$.
14) **end for**
15) **end for**
16) Acquire the WLDM map wC.
17) Compute the mean and maximum values of the WLDM map:

$$mn = \sum_{x=1}^{M}\sum_{y=1}^{N} wC(x,y)/M \times N, sm = \max\{wC(x,y), x \in \{1,\ldots,M\}, y \in \{1,\ldots,N\}\}.$$

18) Acquire the threshold:

$$T = \lambda \cdot sm + (1-\lambda)\cdot mn. \tag{8}$$

19) Segment targets from the WLDM map according to T: A pixel at (x,y) is the target pixel if $wC(x,y) \geq T$ or $wC(x,y) < T$, otherwise it is a background pixel.
20) Achieve the target position.

D. Detection Ability Analysis

From the aforementioned definition, we can find that the multiscale local difference contrast can enhance the target and suppress background clutters and noise. Let (x_0,y_0) be the center pixel point of a target, and its multiscale local difference contrast can be expressed by the following expression, where L is the maximal scale of the current region, Ω_k^t is the kth neighborhood, $k = 1,\ 2,\ldots,L$, and N_k^t is the number of pixels contained in the kth neighborhood, respectively:

$$\begin{aligned}
\widehat{C}^t(x_0,y_0) &= \max\left\{\widehat{C}_1^t, \widehat{C}_2^t, \ldots, \widehat{C}_{L-1}^t, 0\right\} \\
\text{where } \widehat{C}_k^t &= \frac{\left|A_k^t(x_0,y_0) - A_L^t(x_0,y_0)\right|^2}{\left|\alpha_{\max}^t - \alpha_{\min}^t\right|^2} \\
\alpha_{\max}^t &= \max\left\{A_1^t(x_0,y_0), A_2^t \times (x_0,y_0), \ldots, A_L^t(x_0,y_0)\right\} \\
\alpha_{\min}^t &= \min\left\{A_1^t(x_0,y_0), A_2^t \times (x_0,y_0), \ldots, A_L^t(x_0,y_0)\right\} \\
A_k^t(x_0,y_0) &= \frac{1}{N_k^t}\sum_{(s,t)\in\Omega_k^t} f(s,t).
\end{aligned} \tag{9}$$

It is known that a small infrared target that concentrates in a small, homogeneous, and compact area in an image is unrelated to the background in the spatial domain. The background has the correlation in the spatial domain and the stability in the time domain. Consequently, there usually exists discrimination between the target region and neighboring background areas despite that the discrimination is often small.

Moreover, small target shapes are usually assumed as rough circles without anisotropy and prevailing orientations [15]. Then, a small target can be modeled by using a 2-D Gaussian function [32], [33]

$$s(x,y) = A\exp\left[-\frac{1}{2}\left(\left(\frac{x}{\sigma_1}\right)^2 + \left(\frac{y}{\sigma_2}\right)^2\right)\right] \tag{10}$$

where the target $s(x,y)$ is entirely defined by its peak height A and horizontal and vertical extent parameters σ_1 and σ_2,

respectively. Then, for a bright small target, it can be found that

$$A_l^t(x_0, y_0) \geq A_{l+1}^t(x_0, y_0), \text{where } l = 1, 2, \ldots, L-1. \quad (11)$$

Thus

$$\alpha_{\max}^t = A_1^t(x_0, y_0) \qquad \alpha_{\min}^t = A_L^t(x_0, y_0). \quad (12)$$

Therefore

$$\widehat{C}^t(x_0, y_0) \cong 1. \quad (13)$$

For a dark small target, if the current region only involves the target, (11)–(13) are tenable. On the other hand, if the current region includes the target and neighboring background as well, we can find that

$$\begin{aligned} \tilde{A}_l^t(x_0, y_0) &\leq \tilde{A}_{l+1}^t(x_0, y_0), \qquad l = K+1, \ldots, L-1 \\ \tilde{A}_i^t(x_0, y_0) &\leq \tilde{A}_L^t(x_0, y_0), \qquad i = 1, 2, \ldots, K \end{aligned} \quad (14)$$

where K denotes the maximal scale of the target. Then

$$\tilde{\alpha}_{\max}^t = \tilde{A}_L^t(x_0, y_0), \text{and } \tilde{\alpha}_{\min}^t = \tilde{A}_K^t(x_0, y_0). \quad (15)$$

Likewise, the following expression holds for this case:

$$\widehat{\tilde{C}}^t(x_0, y_0) \cong 1. \quad (16)$$

Equations (13)–(16) indicate that the multiscale local difference contrast is more conspicuous in the target region, compared with the original brightness difference in the image. If the maximum window size in (4) is selected appropriately, the value of the multiscale local difference contrast will be close to 1 in the target region.

On the contrary, if the current location is a pixel point in the background, the local mutation between the current region and the neighboring areas is small because the background has the correlation in the spatial domain. Then, the following formula can be warrantable, where A_k^b, $k = 1, 2, \ldots, L$, is the average gray value of the kth neighborhood:

$$A_l^b(x_0, y_0) \cong A_{l+1}^b(x_0, y_0), \text{where } l = 1, 2, \ldots, L-1. \quad (17)$$

Thus

$$\widehat{C}^b(x_0, y_0) \cong 0. \quad (18)$$

In this way, the value of multiscale local difference contrast in the target region is higher than that in the background region. Consequently, the target can be enhanced, and the background can be suppressed effectively. This reveals that the multiscale local difference contrast takes into account the issues of target enhancement and background suppression simultaneously.

However, against an intricate cloudy-sky background, the similar thermal intensity measure between the target and the edges of clouds causes high FAs in the detection of small targets. Compared with the small target, the temperature of clouds is lower, despite the existence of slight discrimination between the target and the clouds. Thus, the brightness of the target is usually greater than that of clouds. The components with high gray levels can be strengthened by using the modified local entropy [30]. This indicates that the target can be enhanced via the modified local entropy.

Accordingly, the WLDM that combines the multiscale local difference contrast with the modified local entropy can separate true targets from jamming objects like edges of clouds, and it considers the problems of target enhancement and background suppression at the same time. Consequently, the WLDM-based small target detection method can work well for small target images against diverse intricate cloudy-sky backgrounds.

III. Experimental Results

In this section, we first introduce the evaluation metrics, baseline methods, and data for comparison. Then, we use five real small target image sequences against different intricate cloudy-sky backgrounds to demonstrate the effectiveness and practicality of the proposed method.

A. Metrics, Baseline Methods, and Data

Both the PD and the FA are helpful to evaluate the detection performance of various small target detection methods [1], [34]. PD denotes the probability of detected targets in multiframe images where targets truly exist, while FA denotes the rate of detected targets in multiframe images where targets do not exist. PD and FA are described as follows [1]:

$$\begin{aligned} \text{PD} &= \frac{\#\text{true detections}}{\#\text{actual targets}} \\ \text{FA} &= \frac{\#\text{false detections}}{\#\text{images}}. \end{aligned} \quad (19)$$

SCR [1] and BSF [30] can also be used to represent the difficulty degree of small target detection. As a general rule, the higher the SCR and BSF values of a small target image are, the easier the targets can be detected. The SCR and BSF are defined as

$$\begin{aligned} \text{SCR} &= \frac{|m_t - m_b|}{\sigma_b} \\ \text{BSF} &= \frac{\sigma_I}{\sigma_O} \end{aligned} \quad (20)$$

where m_t denotes the average gray value of the target, m_b and σ_b denote the average and standard deviation of gray values in the neighboring area around the target, and σ_I and σ_O denote the standard deviations of gray values in the original and filtered images, respectively.

Since the main viewpoint of our method is to represent the local mutation of an image owing to the appearance of a small target, we choose some local difference/mutation descriptors as three baseline methods, including the LMWIE [30], the AGADM [31], and the LCM [2]. Moreover, the top-hat filter (THT) [8], the maximum background prediction model (MBPM) [35], the Maxmean filter, and the Maxmedian filter [22] are also chosen as the baseline methods in this paper.

We use five real small infrared target image sequences (more than 460 images) with low SCR values to compare the proposed methods with the baseline methods, denoted as Real Sequences 1 to 5. The details about targets and backgrounds are listed in Table I.

TABLE I
DETAILS OF FIVE REAL SMALL INFRARED TARGET IMAGE SEQUENCES AGAINST COMPLEX AND NOISY CLOUDY-SKY BACKGROUNDS

	# Frame	Image Resolution	Target Size	Target Shape	Target Details	Background Details
Real Sequence 1	101	460×620	6×4	Circular	✧ A long imaging distance. ✧ A small size with little changing. ✧ Keeping little motion.	✧ Blurred cloudy-sky background. ✧ Changing backgrounds. ✧ Relatively homogeneous.
Real Sequence 2	100	460×620	5×4	Circular	✧ A long imaging distance. ✧ Low SCR value. ✧ Keeping little motion.	✧ Changing backgrounds. ✧ Heavy cloudy-sky background clutters. ✧ Heavy noise.
Real Sequence 3	101	460×620	9×4 to 12×6	Rectangular	✧ A long imaging distance. ✧ A changing size within a small range. ✧ Keeping a little motion.	✧ Changing backgrounds. ✧ Heavy cloudy-sky background clutters.
Real Sequence 4	90	460×620	7×5	Circular	✧ A long imaging distance. ✧ Low SCR value. ✧ Keeping little motion.	✧ Changing backgrounds. ✧ Heavy cloudy-sky background clutters. ✧ Heavy noise.
Real Sequence 5	70	200×256	4×6 to 6×15	Rectangular	✧ A long imaging distance. ✧ A changing size within a big range. ✧ Keeping motion.	✧ Heavy cloudy-sky background clutters to uniform backgrounds. ✧ Heavy noise.

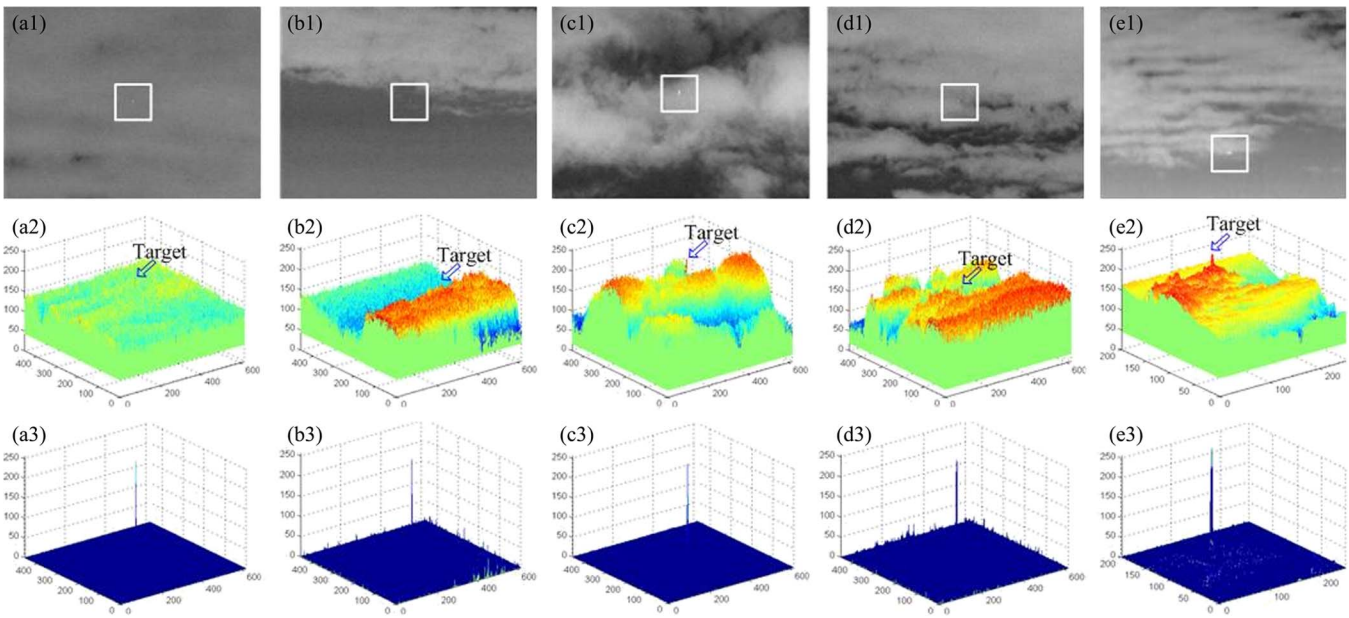

Fig. 2. Target enhancement. (a1)–(e1) Original small infrared target images against different cloudy-sky backgrounds. (a2)–(e2) Three-dimensional gray distributions of (a1)–(e1). (a3)–(d3) Three-dimensional gray distributions of the enhanced results obtained by using our method.

B. Target Enhancement

The base of small target detection is to efficiently suppress background clutters and noise and then enhance the target [8]. Less clutter and noise residual are indispensable to hold lower FAs under the same PD [1]. Thus, if our method can eliminate more background clutters and noise and enhance the small target better, the target can be detected more readily. More than 460 small infrared target images against different cloudy-sky backgrounds are used to verify the performance of our method for target enhancement. Some results are shown in Fig. 2.

Fig. 2(a1)–(e1) are five representative small target images randomly derived from the five real sequences, where the gray value ranges of these images are normalized to [0, 255]. The white squares in Fig. 2(a1)–(e1) indicate the location of the target. The 3-D gray distributions of original images are shown in Fig. 2(a2)–(e2), where the targets are labeled by arrows. It can be found that there are heavy background clutters and noise existed in the original images. However, after our method, the clutters and noise are well suppressed, and the targets are well enhanced, as shown in Fig. 2(a3)–(e3) that displays the 3-D gray distributions of enhanced results. From Fig. 2, we can see that a great deal of background clutters and noise are removed, which suggests that the targets can be easily detected.

The WLDM-based small target detection method is a local gray statistics-based method. However, this type of method is simple, pixelwise, and generally sensitive to noise. In order to demonstrate the performance of the WLDM-based method for noisy images, the five images [i.e., Fig. 2(a1)–(e1)] are added a zero-mean Gaussian white noise, as shown in Fig. 3(a1)–(e1), respectively. According to Table I, there exists heavy noise in Real Sequences 2, 4, and 5. Then, the variances of the added noise in Fig. 3(b1), (d1), and (e1) are 0.002, 0.002, and 0.0005, and others in Fig. 3(a1) and (c1) are 0.003. Through the WLDM, 3-D gray distributions of filtered results are shown in

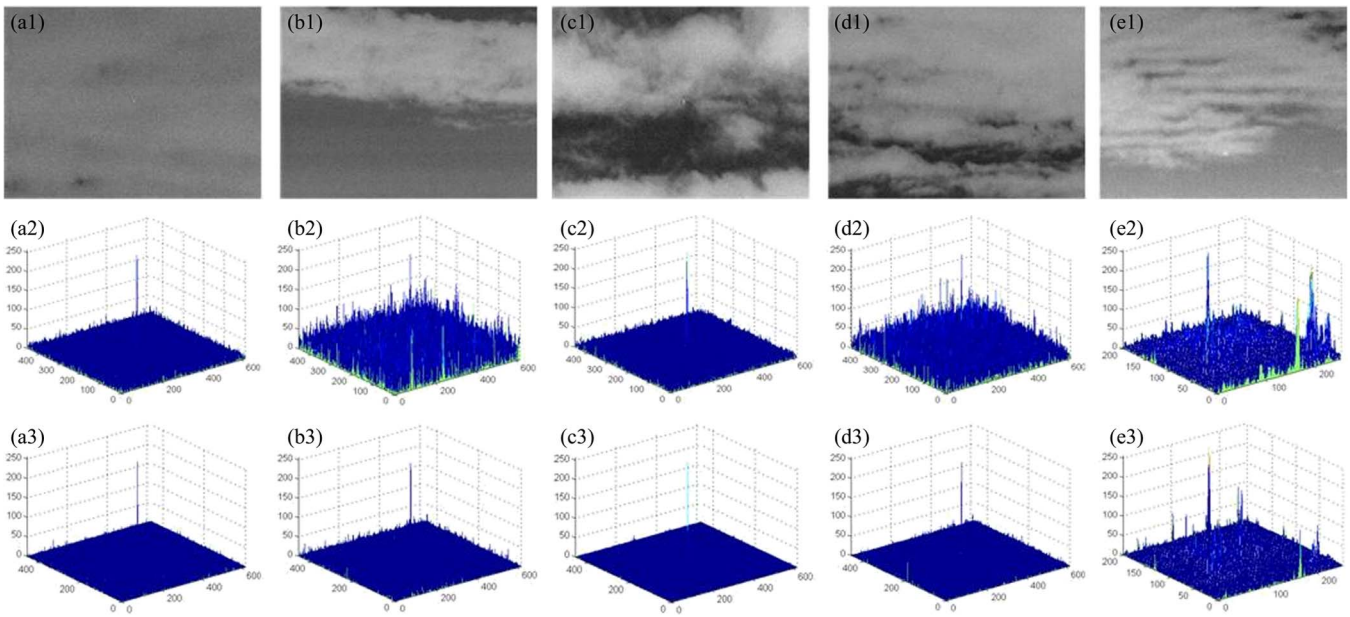

Fig. 3. (a1)–(e1) Noise-added images of Fig. 2(a1)–(e1). (a2)–(e2) Three-dimensional gray distributions of the multiscale local difference contrast map. (a3)–(e3) Three-dimensional gray distributions of the WLDM map.

TABLE II
SCR VALUES OF FIGS. 2 AND 3

Fig. 2	(a1)	(b1)	(c1)	(d1)	(e1)
	3.5386	1.2379	1.8252	1.8924	2.1150
	(a3)	(b3)	(c3)	(d3)	(e3)
	49.9916	12.6613	35.1109	35.8392	39.8300
Fig. 3	(a1)	(b1)	(c1)	(d1)	(e1)
	1.8153	1.0626	1.6554	1.3038	1.9992
	(a2)	(b2)	(c2)	(d2)	(e2)
	15.0532	4.3198	20.2695	7.4656	9.8422
	(a3)	(b3)	(c3)	(d3)	(e3)
	33.8729	7.6821	26.9585	14.2377	20.8923

Fig. 3(a3)–(e3). We can see that the targets in noisy images are well enhanced as well.

The proposed WLDM scheme can be simply described as the multiscale local difference contrast added by the weight-based filtering. For the noise-added images, Fig. 3(a2)–(e2) shows the 3-D gray distributions of filtered results obtained only by using the multiscale local difference contrast. It can be seen that Fig. 3(a2)–(e2) have more clutters and noise residual. However, by means of the weight-based filtering, the clutters and noise residual can be greatly eliminated, as shown in Fig. 3(a3)–(e3). This indicates that the WLDM is insensitive to noise. The same conclusion can also be derived from Table II that lists the SCR values of the original and filtered images with or without added noise. Fig. 3 and Table II suggest that the WLDM can improve the performance of the multiscale local difference contrast to a great extent.

Moreover, two parameters should be pondered reasonably, viz., the maximum window size to compute the multiscale local difference contrast in (4) and the window size to calculate the weights in (6). For Fig. 3(e1), we fix the window size in (6) as 5×5 and set the maximum window size in (4) as 5×5, 7×7, 9×9, 11×11, and 13×13, and then, we test the proposed method, respectively. Table III lists the elapsed time and SCR values of the filtered results. The experiments were

TABLE III
SCR VALUES AND ELAPSED TIME WITH DIFFERENT MAXIMUM WINDOW SIZES IN COMPUTATION OF MULTISCALE LOCAL DIFFERENCE CONTRAST

Size	5×5	7×7	9×9	11×11	13×13
Time	3.2647s	4.2272s	5.3206s	6.6543s	7.8688s
SCR	18.5207	19.6028	20.8923	18.6565	16.9396

conducted on a computer with 8-GB random access memory and Intel Xeon CPU E5-2407, 2.40-GHz processor, and the code was implemented in MATLAB. Considering the SCR as well as the elapsed time, the maximum window size to calculate the multiscale local difference contrast in (4) is chosen as 9×9 (viz., L is equal to 4) in the experiments.

If we fix the maximum window size in (4) as 9×9 and set the window size in (6) as 3×3, 5×5, 7×7, 9×9, and 11×11, the filtered results of Fig. 3(e1) are shown in Fig. 4(a)–(e), respectively. Comparing Fig. 4(a)–(e), it can be seen that the window size of 5×5 results in less clutters and noise residual. Accordingly, the window size to compute the weights in (6) is set as 5×5 (viz., $m = n = 2$) in the experiments.

C. Enhancement Performance Comparison

In order to further verify the enhancement performance of our method, some baseline methods, including THT, LMWIE, MBPM, AGADM, LCM, Maxmean, and Maxmedian methods, are applied on small target images against different complex and noisy backgrounds to do the comparison. Some comparison results are displayed in Fig. 5 and Tables IV and V.

For Fig. 2(a1)–(e1), Fig. 5 denotes the 3-D gray distributions of enhanced results obtained by using various baseline methods. Some weak targets are well enhanced in Fig. 5(c4)–(c7) and (e1)–(e7). However, it can be seen that there exist much clutters and noise residual in those results. Comparing Fig. 2 with Fig. 5, we can see that our method produces less clutters and noise residual for diverse complex and noisy backgrounds. This

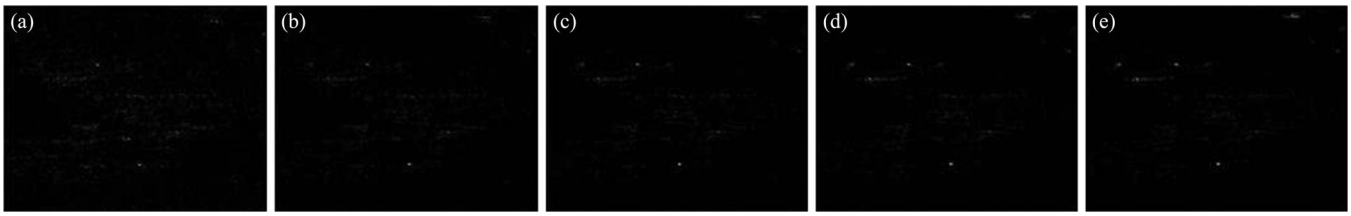

Fig. 4. Filtered results of Fig. 3(e1) with different window sizes in (6) when the maximum window size in (4) is set as 9×9. (a) 3×3. (b) 5×5. (c) 7×7. (d) 9×9. (e) 11×11.

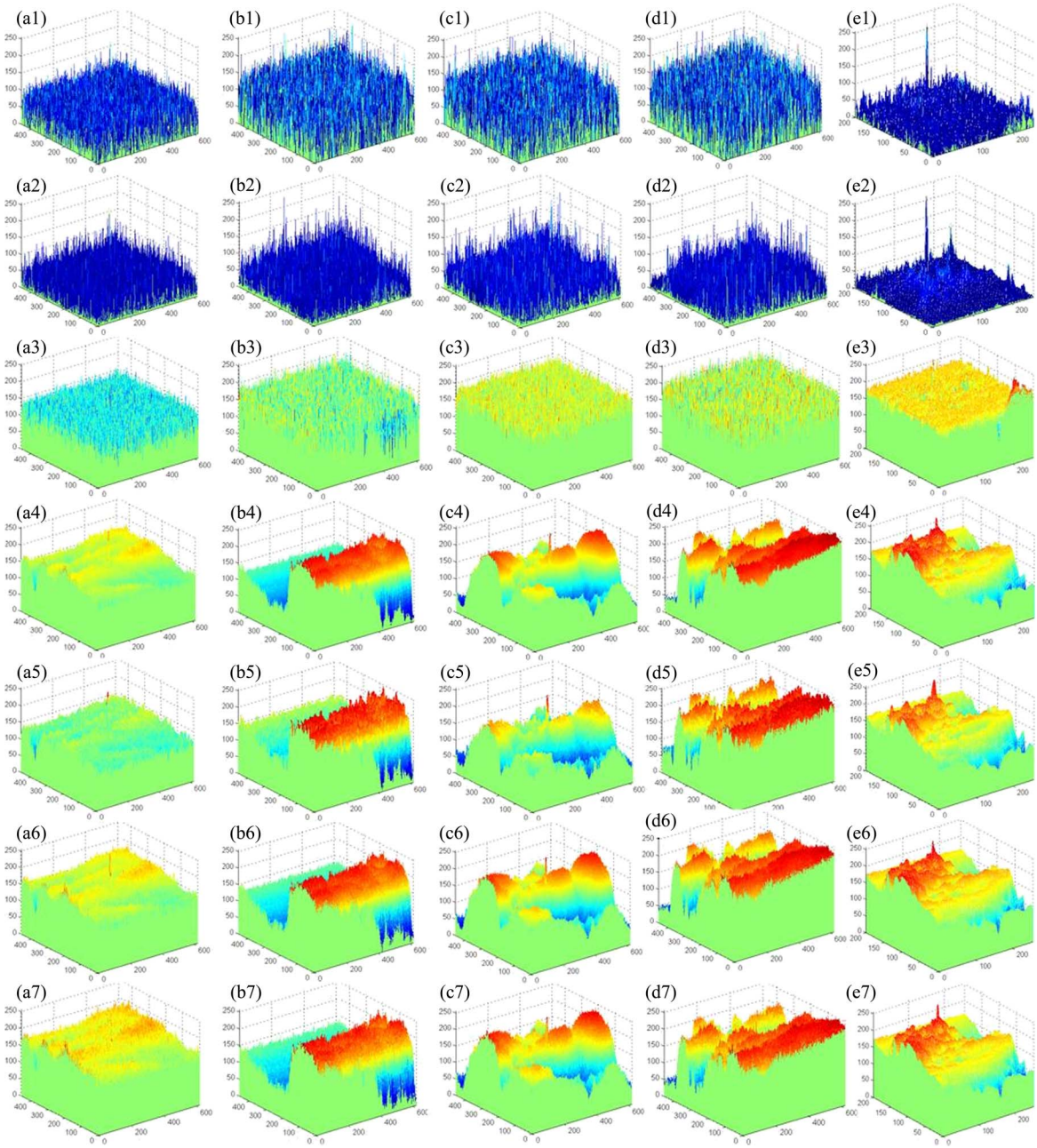

Fig. 5. Enhanced results obtained through different baseline methods. (a1)–(e1), (a2)–(e2), (a3)–(e3), (a4)–(e4), (a5)–(e5), (a6)–(e6), and (a7)–(e7) Enhanced results obtained by using the THT, LMWIE, MBPM, AGADM, LCM, Maxmean, and Maxmedian methods, respectively.

indicates that our method can achieve lower FAs under the same PD.

Against an intricate cloudy-sky background, small targets generally submerge in the clutters and noise. Nevertheless, the target area is different from the surrounding clutters and noise in the spatial domain. This difference is the foundation of our method that intends to amplify the difference between the target and neighboring backgrounds. Thus, our method can efficiently discriminate the target from the background clutters and noise by availably suppressing the complex backgrounds. Figs. 2 and 5 indicate that our method can easily detect small targets and perform better than baseline methods.

TABLE IV
SCR VALUES OF FIVE GROUPS OF ORIGINAL AND FILTERED IMAGES OBTAINED BY USING DIFFERENT METHODS

Group	# 1	# 2	# 3	# 4	# 5
Original	3.2580	1.1586	2.3031	1.5153	1.7140
THT	0.8227	0.4967	0.9185	0.7588	1.0970
LMWIE	1.4421	0.4391	1.4149	0.5808	0.9672
MBPM	10.4830	1.9836	2.3015	1.7662	1.6090
AGADM	3.8688	1.1711	9.1863	2.4599	7.8038
LCM	8.2449	4.4570	4.8562	2.7402	2.1123
Maxmean	7.8871	1.9075	2.4337	1.8175	1.7011
Maxmedian	6.6161	1.5707	2.5811	1.7299	1.6695
Our method	45 7002	12 3978	38 1118	38 6720	34 0139

TABLE V
BSF VALUES OF FILTERED RESULTS OBTAINED BY USING DIFFERENT METHODS

Real Sequence	# 1	# 2	# 3	# 4	# 5	Average
THT	0.32	0.79	1.77	0.84	3.94	1.53
LMWIE	0.75	2.10	5.09	2.24	5.54	3.14
MBPM	0.48	1.19	2.92	1.30	2.82	1.74
AGADM	0.56	0.52	0.72	0.56	0.57	0.59
LCM	0.65	0.61	0.96	0.61	0.70	0.71
Maxmean	0.54	0.54	0.75	0.58	0.60	0.60
Maxmedian	0.55	0.55	0.76	0.59	0.60	0.61
Our method	12.55	15.43	45.48	31.96	11.16	23.32

SCR and BSF are appropriate measures to demonstrate the detection performance of diverse methods and are used here for comparison. For each measure, a higher score means the better performance. Five groups of images are randomly selected from the five small target image sequences, denoted as Groups 1 to 5. Each group contains successive eight images. Table IV list the average SCR values of the five groups of the original and filtered images obtained by using the THT, LMWIE, MBPM, AGADM, LCM, Maxmean, Maxmedian, and proposed methods. It can be found that our method can significantly improve the SCR values of the images.

Table V shows the average BSF values of the five real image sequences. More than 460 images are used to calculate the ensemble average BSF values obtained by using the baseline and proposed methods, listed in the right column of Table V. According to Tables IV and V, our method shows superiority over the baseline methods in terms of the SCR values and BSF values. This is because our method can availably suppress diverse complex and noisy backgrounds and has less clutters and noise residual in the comparison of Figs. 2–5.

These experimental results demonstrate the performance of our method for target enhancement and background clutter and noise suppression simultaneously. Therefore, our method is helpful to detect small infrared targets embedded in different heavy and noisy cloudy-sky background clutters.

D. Target Detection

Generally, if the distance between centers of the ground truth of the target location and the detected result is in a threshold (5 pixels [4], 4 pixels [2], or others), the detected result will be considered correct. In this paper, the threshold is selected as 4 pixels. For the five small target sequences, the probabilities of detection obtained by using our method are 1.00, 0.79, 1.00, 1.00, and 1.00, and the FAs are 0.0198, 0.4100, 0.0198, 0.0444, and 0.0286, respectively, where the parameter λ in (8) was

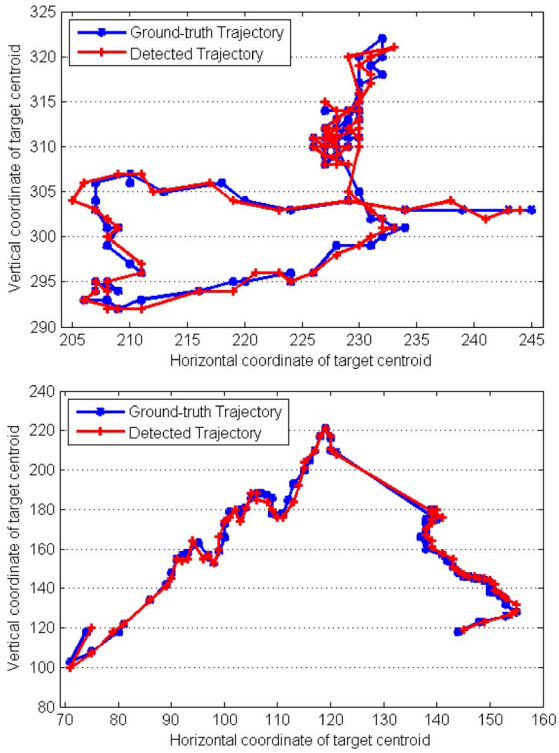

Fig. 6. Ground-truth and detected trajectories based on our method. (a) Real Sequence 3. (b) Real Sequence 5.

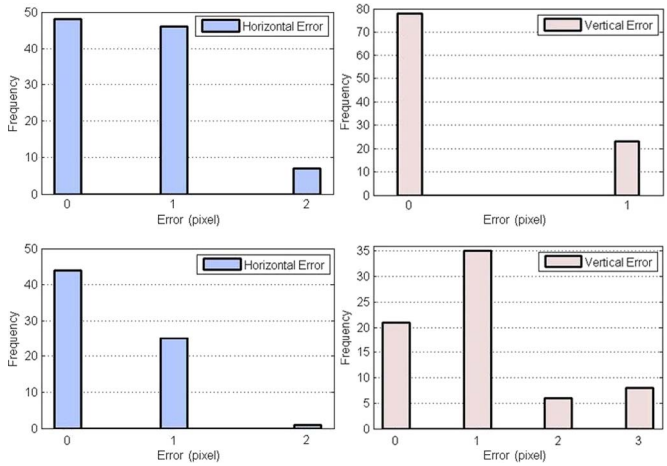

Fig. 7. Histograms of detected error distributions of (upper) Real Sequence 3 and (lower) Real Sequence 5.

selected as 0.3, 0.6, 0.3, 0.4, and 0.4 in each experiment. These results suggest that our method can achieve high probabilities of detection and low FAs.

In Real Sequences 3 and 5, the targets keep motion in each frame, while the targets in Real Sequences 1, 2, and 4 have little motion (see Table I). For Real Sequences 3 and 5, Fig. 6 shows the ground-truth and detected trajectories obtained by using our method, and Fig. 7 shows the corresponding histograms of error distributions. In Fig. 6(a), the tracked trace does almost match that of the target movement. It can be observed from the upper row of Fig. 7 that the most horizontal errors are less than 1 pixel and the vertical errors are less than 1 pixel. The tracked trace in Fig. 6(b) also does almost match that of the target movement. The major horizontal errors are less than 1 pixel, and the major vertical errors are less than 2 pixels (see Fig. 7).

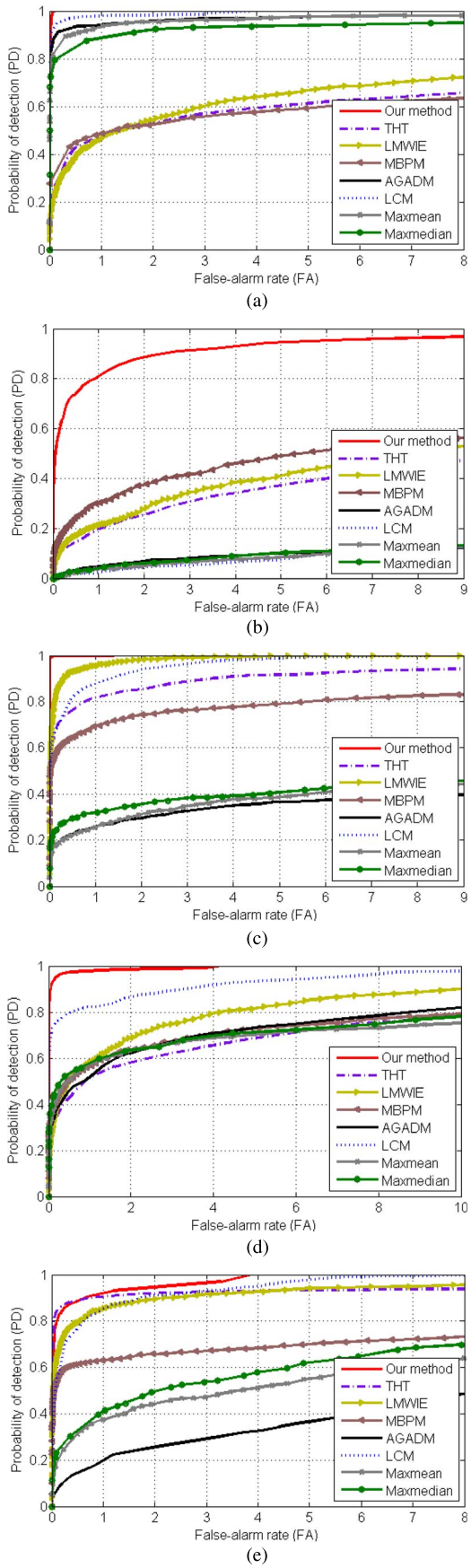

Fig. 8. ROC curves of eight methods for five real infrared image sequences. (a) Real Sequence 1. (b) Real Sequence 2. (c) Real Sequence 3. (d) Real Sequence 4. (e) Real Sequence 5.

E. Detection Performance Comparison

The receiver operating characteristic (ROC) curve is a plot of the true PD versus the FA. We give the ROC curves of the eight methods for the five real small target image sequences in Fig. 8. The PD and the FA are based on (19). ROC curves suggest that our method has better performance wrt detection accuracy than baseline methods. Particularly for Real Sequences 1 to 4, our method owns higher values of PD but lower values of FA, compared with the baseline methods. For Real Sequences 1, 3, and 4, the LCM method is superior to other baseline methods. but for Real Sequence 2, the LCM method has very low values of PD. For Real Sequence 5, the THT method have a little better performance than our method when FA ≤ 0.7, but our method can reach 1 (100%) faster than that baseline method when FA > 0.7. Therefore, our method can obtain the best performance for the five small infrared target image sequences, which implies that our method works more robustly for various clutter and noisy backgrounds and target movements.

IV. Conclusion

This paper presents an effective method based on a WLDM to detect small infrared targets against diverse intricate cloudy-sky backgrounds. The method weights the multiscale local difference contrast by the modified local entropy followed by a simple adaptive threshold operation. It can separate the true target from jamming objects (e.g., edges of clouds) that have a similar thermal intensity measure wrt the background as small targets in the scene. The presented method can eliminate massive intricate cloudy-sky background clutters and noise through the target enhancement. In particular, it can significantly improve the SCR and BSF values of the image. In this way, the presented method can achieve high probabilities of detection and low FAs. Experiments implemented on extensive small target images against diverse complicated cloudy-sky background clutters demonstrate that our method significantly outperforms classical methods, such as the THT, LMWIE, MBPM, AGADM, LCM, Maxmean, and Maxmedian. Experimental results also demonstrate that our method works stably for different intricate backgrounds and target movements. In the future, we will investigate a faster version of the current algorithm. We will also further improve the flexibility of our method in background cases with heavy interference of the cloud edge texture and noise (e.g., Real Sequence 2) in our further investigation.

References

[1] C. Q. Gao *et al.*, "Infrared patch-image model for small target detection in a single image," *IEEE Trans. Image Process.*, vol. 22, no. 12, pp. 4996–5009, Dec. 2013.

[2] C. L. Philip *et al.*, "A local contrast method for small infrared target detection," *IEEE Trans. Geosci. Remote Sens.*, vol. 51, no. 1, pp. 574–581, Jan. 2014.

[3] M. Malanowski and K. Kulpa, "Detection of moving targets with continuous-wave noise radar: Theory and measurements," *IEEE Trans. Geosci. Remote Sens.*, vol. 50, no. 9, pp. 3502–3509, Sep. 2012.

[4] S. Kim and J. Lee, "Scale invariant small target detection by optimizing signal-to-clutter ratio in heterogeneous background for infrared search and track," *Pattern Recognit.*, vol. 45, no. 1, pp. 393–406, Jan. 2012.

[5] H. Deng, Y. T. Wei, and M. W. Tong, "Small target detection based on weighted self-information map," *Infrared Phys. Technol.*, vol. 60, pp. 197–206, Sep. 2013.
[6] N. Thanh, H. Sahli, and D. Hao, "Infrared thermography for buried landmine detection: Inverse problem setting," *IEEE Trans. Geosci. Remote Sens.*, vol. 46, no. 12, pp. 3987–4504, Dec. 2008.
[7] B. Porat and B. Friendlander, "A frequency domain algorithm for multiframe detection and estimation of dim targets," *IEEE Trans. Pattern Anal. Mach. Intell.*, vol. 12, no. 4, pp. 398–401, Apr. 1990.
[8] X. Z. Bai and F. G. Zhou, "Analysis of new top-hat transformation and the application for infrared dim small target detection," *Pattern Recognit.*, vol. 43, no. 6, pp. 2145–2156, Jun. 2010.
[9] C. Q. Gao, T. Q. Zhang, and Q. Li, "Small infrared target detection using sparse ring representation," *IEEE Trans. Aerosp. Electron. Syst.*, vol. 27, no. 3, pp. 21–30, Mar. 2012.
[10] H. Deng, J. G. Liu, and H. Li, "EMD based infrared image target detection method," *J. Infrared Millim. W.*, vol. 30, no. 11, pp. 1205–1215, Jul. 2009.
[11] P. L. Shui, D. C. Li, and S. W. Xu, "Tri-feature-based detection of floating small targets in sea clutter," *IEEE Trans. Aerosp. Electron. Syst.*, vol. 50, no. 2, pp. 1416–1430, Apr. 2014.
[12] Y. F. Gu, C. Wang, B. X. Liu, and Y. Zhang, "A kernel-based nonparametric regression method for clutter removal in infrared small-target detection application," *IEEE Geosci. Remote Sens. Lett.*, vol. 7, no. 3, pp. 469–473, Jul. 2010.
[13] I. S. Reed, R. M. Gagliardi, and L. B. Stotts, "Optical moving target detection with 3D matched filtering," *IEEE Trans. Aerosp. Electron. Syst*, vol. 24, no. 4, pp. 327–336, Jan. 1988.
[14] M. Li, T. Zhang, W. Yang, and X. Sun, "Moving weak point target detection and estimation with three-dimensional double directional filter in IR cluttered background," *Opt. Eng.*, vol. 44, Oct. 2005, Art. no. 107007.
[15] X. Liu and Z. Zuo, *A Dim Small Infrared Moving Target Detection Algorithm Based on Improved Three-Dimensional Directional Filtering Communications in Computer and Information Science*, vol. 363. New York, NY, USA: Springer-Verlag, 2013, ch. 13, pp. 102–108.
[16] Z. Wang, J. Tian, J. Liu, and S. Zhen, "Small infrared target fusion detection based on support vector machines in the wavelet domain," *Opt. Eng.*, vol. 45, no. 7, Jul. 2006, Art. no. 076401.
[17] B. Zhang, T. Zhang, Z. Cao, and K. Zhang, "Fast new small-target detection algorithm based on a modified partial differential equation in infrared clutter," *Opt. Eng.*, vol. 46, no. 10, Oct. 2007, Art. no. 106401.
[18] H. Deng, J. G. Liu, and Z. Chen, "Infrared small target detection based on modified local entropy and EMD," *Chin. Opt. Lett.*, vol. 8, no. 1, pp. 24–28, Jan. 2010.
[19] S. Kim and J. Lee, "Small Infrared target detection by region-adaptive clutter rejection for sea-based infrared search and track," *Sersors (Basel)*, vol. 14, no. 7, pp. 13210–42, Jul. 2014.
[20] J. J. Soraghan, "Small-target detection in sea clutter," *IEEE Trans. Geosci. Remote Sens.*, vol. 42, no. 7, pp. 1355–1361, Jul. 2004.
[21] S. C. Pohlig, "Spatial-temporal detection of electro-optic moving targets," *IEEE Trans. Aerosp. Electron. Syst.*, vol. 31, no. 2, pp. 608–616, Apr. 1995.
[22] S. Deshpande, M. Er, and R. Venkateswarlu, "Maxmean and Maxmedian filters for detection of small-targets," in *Proc. SPIE*, Oct. 1999, vol. 3809, pp. 74–83.
[23] J. Guan, X. L. Chen, Y. Huang, and Y. He, "Adaptive fractional Fourier transform-based detection algorithm for moving target in heavy sea clutter," *IET Radar Sonar Navig.*, vol. 6, no. 5, pp. 389–401, Jun. 2011.
[24] X. L. Chen, J. Guan, N. B. Liu, and Y. He, "Maneuvering target detection via Radon-fractional Fourier transform-based long-time coherent integration," *IEEE Trans. Signal Process.*, vol. 62, no. 4, pp. 939–953, Jan. 2014.
[25] H. Li, Y. Wei, L. Li, and Y. Y. Tang, "Infrared moving target detection and tracking based on tensor locality preserving projection," *Infrared Phys. Technol.*, vol. 53, no. 2, pp. 77–83, Mar. 2010.
[26] M. Shirvaikar and M. Trivedi, "A neural network filter to detection small targets in high background clutters," *IEEE Trans Neural Netw.*, vol. 6, no. 1, pp. 252–257, Jan. 1995.
[27] J. F. Khan and M. S. Alam, "Target detection in cluttered forward-looking infrared imagery," *Opt. Eng.*, vol. 44, no. 7, Jul. 2005, Art. no. 076404.
[28] D. Song and D. Tao, "Biologically inspired feature manifold for scene classification," *IEEE Trans. Image Process.*, vol. 19, no. 1, pp. 174–184, Jan. 2010.
[29] Y. Gao, R. Liu, and J. Yang, "Small target detection using two-dimensional least mean square (TDLMS) filter based on neighborhood analysis," *J. Infrared Millim. W.*, vol. 29, no. 2, pp. 188–200, Feb. 2008.
[30] X. J. Qu, H. Chen, and G. H. Peng, "Novel detection method for infrared small targets using weighted information entropy," *J. Syst. Eng. Electron.*, vol. 23, no. 6, pp. 838–842, Dec. 2012.
[31] G. Y. Wang, T. X. Zhang, L. G. Wei, and N. Sang, "Efficient method for multiscale small target detection from a natural scene," *Opt. Eng.*, vol. 35, no. 3, pp. 761–768, Mar. 1996.
[32] K. L. Anderson and R. A. Iltis, "A tracking algorithm for infrared image based on reduced sufficient statistics," *IEEE Trans. Aerosp. Electron. Syst.*, vol. 33, no. 2, pp. 464–472, Apr. 1997.
[33] Y. Xiong, J. X. Peng, M. Y. Ding, and D. H. Xue, "An extended track-before-detect algorithm for infrared target detection," *IEEE Trans. Aerosp. Electron. Syst*, vol. 33, no. 3, pp. 1087–1092, Jul. 1997.
[34] J. F. Rivest and R. Fortin, "Detection of dim targets in digital infrared imagery by morphological image processing," *Opt. Eng.*, vol. 35, no. 7, pp. 1886–1893, Jul. 1996.
[35] K. Huang and X. Mao, "Detectability of infrared small targets," *Infr. Phys. Technol.*, vol. 53, no. 3, pp. 208–217, May 2010.

He Deng received the Ph.D. degree in control science and engineering from the Huazhong University of Science and Technology, Wuhan, China in 2011.

He is currently a Postdoctor in the Wuhan Institute of Physics and Mathematics, Chinese Academy of Sciences, Wuhan, China, and he is a Lecturer in the Department of Information Technology, Central China Normal University, Wuhan. His current research interests are target detection and image processing.

Xianping Sun received the B.S. degree from Peking University, Beijing, China.

He is currently a Professor in the Wuhan Institute of Physics and Mathematics, Chinese Academy of Sciences, Wuhan, China. His current research interests include signal acquisition and processing.

Maili Liu received the Ph.D. degree from the University of London, London, U.K.

He is currently a Professor in the Wuhan Institute of Physics and Mathematics, Chinese Academy of Sciences, Wuhan, China. His current research interests include NMR spectroscopy, imaging acquisition, and applications.

Chaohui Ye received the B.S. degree from Peking University, Beijing, China.

He is currently a Professor in the Wuhan Institute of Physics and Mathematics, Chinese Academy of Sciences, Wuhan, China. His current research interests include novel imaging techniques and applications in biomedicine and physics.

Xin Zhou received the Ph.D. degree from the Chinese Academy of Sciences, Wuhan, China.

He is currently a Professor in the Wuhan Institute of Physics and Mathematics, Chinese Academy of Sciences, Wuhan, China. His current research interests are scientific instrument developments, imaging acquisition, and data processing.